AEROSPACE REPORT NO.
ATR-2021-02018

Relativistic Proton Spectrometer Flux Determination and Data Products

September 27, 2021

T. P. O'Brien[1], M. D. Looper[1], J. E. Mazur[2], E. L. Mazur[3]
[1]Space Sciences Department, Space Science Applications Laboratory
[2]Space Science Applications Laboratory, Physical Sciences Laboratories
[3]Sensors and Systems, xLab

Prepared for:

JHU/APL
11100 Johns Hopkins Road
Laurel, MD 20723-6099

Contract No. 135557

Authorized by: Engineering and Technology Group

Acknowledgments

The authors acknowledge many useful discussions with members of the Space Science Applications Laboratory, xLab, and the Van Allen Probes team, and especially S. Claudepierre for peer reviewing this report and assisting in its improvement.

Abstract

The Relativistic Proton Spectrometer (RPS) instrument measures protons with energies from approximately 60 MeV to >1 GeV. It was built to provide high-precision fluxes to the AP9 trapped radiation climatology model. In this report, we describe the processes used to convert sensor data records to particle flux. This process includes background rejection, event energy identification, deadtime and quota correction, flux conversion, and adjustment for on-orbit changes in the instrument itself. We produced our fluxes as level 2 products, which are fluxes in 20 differential energy channels as a function of time along the spin and orbit of the spacecraft and 1-minute averages in each of the channels. From the level 2 spin-resolved fluxes, we produced level 3 products, which are separately accumulated into energy spectra in spin sectors, local pitch angles, and equatorial pitch angles. We also produced level 4 products, which are daily and by-leg flux maps in multiple magnetic drift invariant coordinates.

Contents

Figures

Tables

1. Introduction

The Relativistic Proton Spectrometer (RPS) measures protons with energies from about 60 MeV to >1 GeV. It consists of two front and two back disc solid-state detectors (SSDs) that define the coincidence geometry (the "A" detectors), eight energy-analyzing "D" disc SSDs, and a Cherenkov radiator (the D9 detector). Only two of the A detectors are active in the coincidence scheme at any time, while typically all eight D SSD detectors are active, and the D9 Cherenkov detector is active, but an optional part of the coincidence. Events that trigger the As and D1–D8 are called penetrating (PEN) events, while events that also trigger the Cherenkov radiator are called CHE events. Figure 1 shows a diagram of the sensor as rendered in Geant4 [2].

Energy deposits in D1–D8 and collected charge in D9 are inferred through pulse height analysis and telemetered to the ground in direct event packets. Due to telemetry limitations, RPS has a variable quota on the number of direct events that can be sent every second, with separate quotas for PEN and CHE events. On the ground, the events are analyzed to reject events that are not likely to be protons going forward through the detector stack (i.e., to remove background). Events are then assigned an expected incident proton energy. The events are binned into channels, and the counts in each channel are used to compute a proton spectrum, correcting for quota, sensor deadtime, channel response according to the Geant4 simulation, and on-orbit changes in the sensor performance. This document describes the algorithms used in RPS ground processing that ultimately produces the flux data products for RPS.

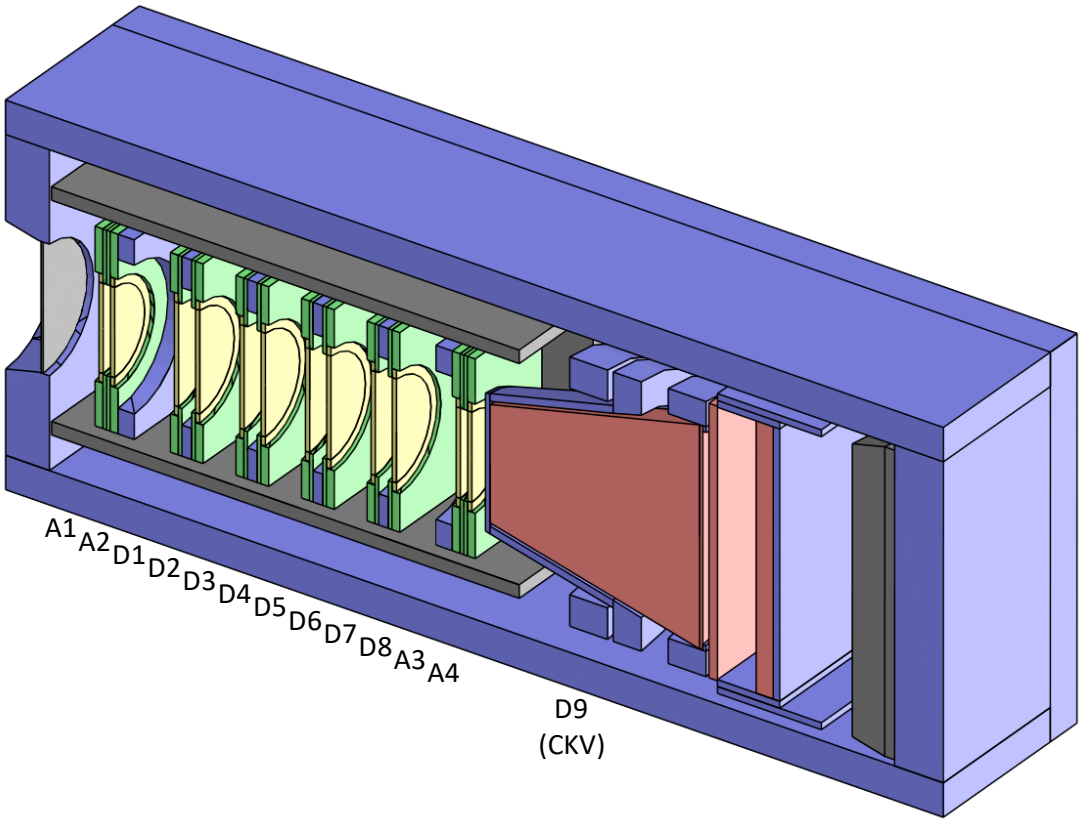

Figure 1. Geant4 rendering of the RPS instrument with SSDs A1–A4, D1–D8, and the Cherenkov radiator D9 indicated. A particle enters from the left. SSDs are indicated in yellow, the Cherenkov radiatior is indicated in maroon. The A detectors are slightly smaller than the D detectors, allowing them to define the sensor field of view while minimizing edge effects in the energy-analyzing D detectors.

2. Conversion to Physical Units

Telemetry unpacking is described in Reference [3]. For the purposes of flux determination, the most essential conversion from telemetry quantities to physical units is conversion from pulse heights in D1–D8 to energy deposit in MeV and conversion from pulse height in D9 to photon counts. Looper et al. [2] describes the simulation and calibration procedures used to obtain the conversion factors, but we repeat the factors and calculations here for completeness.

The SSD conversion from pulse height to energy deposit is a linear transform with a gain and offset, with a divisor that is linear in temperature:

$$D_i = \frac{c_i + H_i g_i}{T_0 + T_1 \bar{T}(t)}$$

$$D_i = \text{Deposit in } i^{\text{th}} \text{ SSD, MeV}$$
$$c_i = \text{Offset for } i^{\text{th}} \text{ SSD, MeV}$$
$$g_i = \text{Gain for } i^{\text{th}} \text{ SSD, MeV/channel}$$
$$H_i = \text{Pulse height for } i^{\text{th}} \text{ SSD}$$
$$T_0 = 1.02 = \text{Temperature correction offset}$$
$$T_1 = -6.22 \times 10^{-4} = \text{Temperature correction slope } 1/^{\circ}\text{C}$$
$$\bar{T}(t) = \text{Daily-averaged temperature, } ^{\circ}\text{C}$$
$$t = \text{time}$$

Table 1 gives two sets of gains and offsets, one from the on-board radioactive alpha source built into each SSD and one from the Geant4 simulation. The EVENT_ENERGY_DEPOSIT values reported in the level 1 and level 2 data files reflect the alpha source values, which, as noted in [2], reflect our best estimate of the true energy deposits. However, for much of this document, it is the simulation-referenced gain and offset values that are used (e.g., for the polygon filters discussed in section 3 and for computing the event energy assignments discussed in section 4).

In addition to the initial linear gain and offset conversions, we correct the energy deposit for temperature effects in the analog-to-digital converter. This temperature correction takes the form of the divisor given above. The temperature $\bar{T}(t)$ is taken from daily average of the DC-DC converter temperature monitor value provided in the instrument housekeeping packets and interpolated to the time of the direct event.

Table 1. Gain and Offset for SSD Conversion from Pulse Height to MeV Energy Deposit

Detector	Alpha Source		Simulation	
	Gain	Offset	Gain	Offset
RPS-A				
D1	0.006463	0.04268	0.006666326	0.05315223
D2	0.006479	0.04484	0.006698962	0.05416242
D3	0.006464	0.04417	0.006725986	0.05165412
D4	0.006477	0.04356	0.006695923	0.05292184
D5	0.006450	0.04407	0.006666139	0.05319168
D6	0.006463	0.04642	0.006674405	0.05324131
D7	0.006470	0.04047	0.006615704	0.05358268
D8	0.006460	0.04459	0.006543851	0.06111138

Detector	Alpha Source		Simulation	
	Gain	Offset	Gain	Offset
RPS-B				
D1	0.006482	0.04911	0.006691855	0.05350441
D2	0.006482	0.05277	0.006735900	0.05782391
D3	0.006523	0.01424	0.006738977	0.02193629
D4	0.006479	0.05312	0.006715937	0.05301029
D5	0.006496	0.04865	0.006667559	0.05332874
D6	0.006483	0.05197	0.006690197	0.05661310
D7	0.006482	0.04964	0.006608464	0.05777105
D8	0.006482	0.04720	0.006569961	0.05809350

The Cherenkov pulse height is converted to photons using a gain and offset as well as two divisors accounting for temperature and temporal drift.

$$D_9 = \frac{c_9 + H_9 g_9}{[1 + X\bar{T}(t)]Y(t)}$$

$$D_9 = \text{Cherenkov photon count}$$
$$c_9 = \text{Offset, photons}$$
$$g_9 = \text{Gain, photons/channel}$$
$$H_i = \text{Pulse height Cherenkov readout}$$
$$X = \text{Temperature coefficient, } 1/°\text{C}$$
$$\bar{T}(t) = \text{Daily-averaged temperature, } °\text{C}$$
$$Y(t) = \text{Drift factor}$$

Table 2 provides the static parameters of the Cherenkov calibration. The drift factor is time dependent and is computed by linear interpolation and extrapolation from the following fixed arrays. For RPS-A, $Y(t)$ takes values of 0.898, 1.013, 1.013, 0.930, 0.884, and 0.855 at corresponding fiducial decimal year points 2012.75, 2012.8, 2012.9, 2013.9, 2014.9, and 2016.0. For RPS-B, $Y(t)$ takes values of 0.947, 0.976, 0.976, 0.867, and 0.779 at corresponding fiducial decimal year points 2012.75, 2013.0, 2013.5, 2016.5, and 2019.5. As with other calibration factors given here, the process for determining $Y(t)$ corrections are given in [2].

Table 2. Cherenkov Calibration Factors

Parameter	RPS-A	RPS-B
c_9	7.42765	8.705149
g_9	2.649163	0.7694737
X	-0.015	-0.02

3. Background Rejection

Aside from the eight-fold and nine-fold coincidence required to initiate on-board event processing and downlink, we also apply two polygon cuts in the ground processing. It is important to note that the polygon filters use the SSD energy deposits calibrated to the simulations, not those calibrated to the alpha source deposits. The first cut removes fully coincident, but low-energy backward-going protons. The second cut removes higher-energy backward-going protons and other high-energy particles.

As described in [2], the first cut is in the (D1, D8) domain, shown in Figure 2. We define a polygon in D1–D8 space and determine whether a given event is within the polygon. The polygon check is done in log-log space, as depicted in the figure. Points outside the polygon are marked as backward (or, at least, not forward). The polygon vertices in $\log_{10} X$ are 0.27, 0.27, 0.345, 0.5, 0.7, 1.0, 1.3, 1.6, 2.0, 2.25, 2.45, 3.25, 3.25, 3.15, 2.8, 1.5, 1.0, 0.46, 0.34, and 0.29. The polygon vertices in $\log_{10} Y$ are 0.29, 0.36, 0.475, 1.1, 1.55, 2.0, 2.4, 3.0, 4.3, 6.0, 10.0, 10.0, 6.5, 4.5, 3.0, 0.75, 0.5, 0.34, 0.27, and 0.27. The main set of particles rejected is backward protons that slow down significantly in the detector stack and therefore deposit more energy in D1 than in D8.

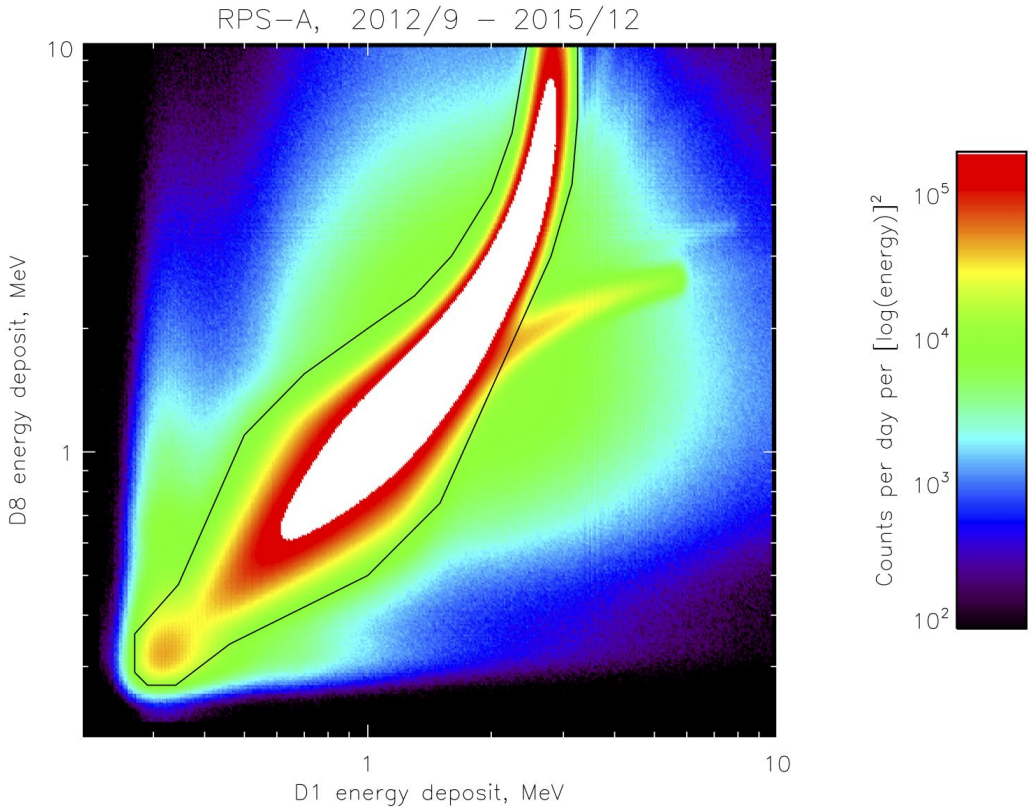

Figure 2. D1–D8 polygon cuts that mainly remove backward-going protons at the low-energy end of the RPS response (those that deposit more in D1 than in D8 as they slow down in the detector stack). Points outside the polygon are considered backward, or, at least, not forward.

The second cut we apply is in MIN2SSD-Cherenkov space. MIN2SSD is the average of the minimum two deposits in the *D* detectors. Figure 3 shows an example of this cut, which is affectionately known as the Nessie plot, after the Loch Ness monster. Nessie's neck is the main response of relativistic protons: as

their energy increases, they produce more Cherenkov light, up to saturation at fully relativistic energies (approximate GeV) in Nessie's head. Nessie's body and back are made up of scintillation in the Cherenkov radiator. Backward protons, helium and other particle species appear as other concentrations of particles in this domain outside the polygon. The polygon vertices in $\log_{10} X$ are 0.50, 0.44, 0.42, 0.41, 0.375, 0.335, 0.30, 0.27, 0.26, 0.26, 0.28, 0.31, 0.34, 0.385, 0.44, 0.50, 0.90, 3.15, and 3.15. The polygon vertices in $\log_{10} Y$ are 0.1, 17, 30, 70, 180, 315, 400, 440, 480, 590, 680, 680, 520, 390, 250, 90, 110, 65, and 0.1. As shown in the figure, the polygon filter is applied in a log-log sense.

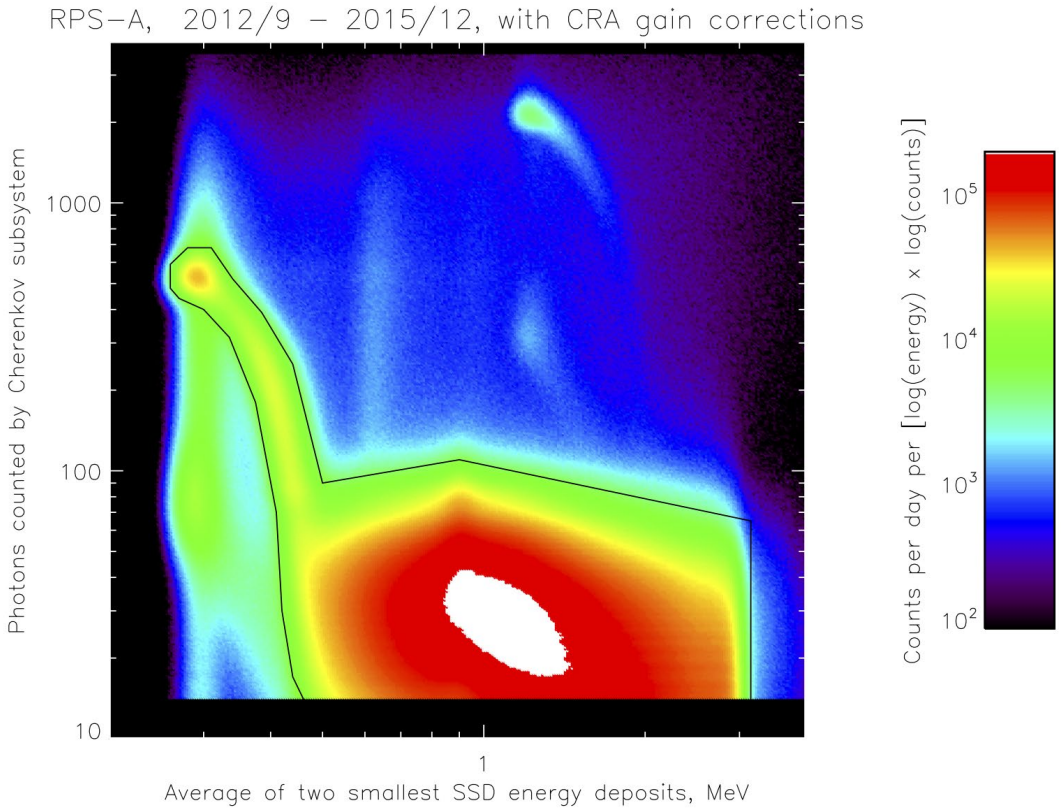

Figure 3. Cherenkov vs. MIN2SSD cuts, the so-called Nessie plot. These cuts remove high-energy particles and non-proton backgrounds. Points outside the polygon are considered backward or, at least, not forward.

These two polygon filters are used to assign the EVENT_DIRECTION, which is present in the level 1 and level 2 files. Events that are inside both polygons are given a forward direction (0), and all other events are given a backward direction (1).

4. Proton Energy Assignment

Over the course of the RPS mission, we tried several different schemes for energy assignment. In the instrument paper [4], we described a nearest-neighbors look-up method, dubbed "enigma," but that proved too slow for routine processing. Ultimately, we settled on an analytical formula related to the average of the minimum two SSD deposits (MIN2SSD). Across all the energy assignment methods we tried, the energy resolution diminishes as the incident energy approaches one GeV. Figure 1 shows the simulation and fit for the MIN2SSD energy assignment approach.

$$\log_{10} E_{MIN2SSD}(\text{MeV}) = a_4 x^4 + a_3 x^3 + a_2 x^2 + a_1 x + a_0$$
$$x = \log_{10} \frac{S_1 + S_2}{2}(\text{MeV})$$
$$a_0 = 2.1548248732$$
$$a_1 = -1.2773856886$$
$$a_2 = 0.52673691466$$
$$a_3 = 1.8930410283$$
$$a_4 = -10.501081252$$
$$S_1 = \text{Smallest SSD deposit, MeV}$$
$$S_2 = \text{Second smallest SSD deposit, MeV}$$

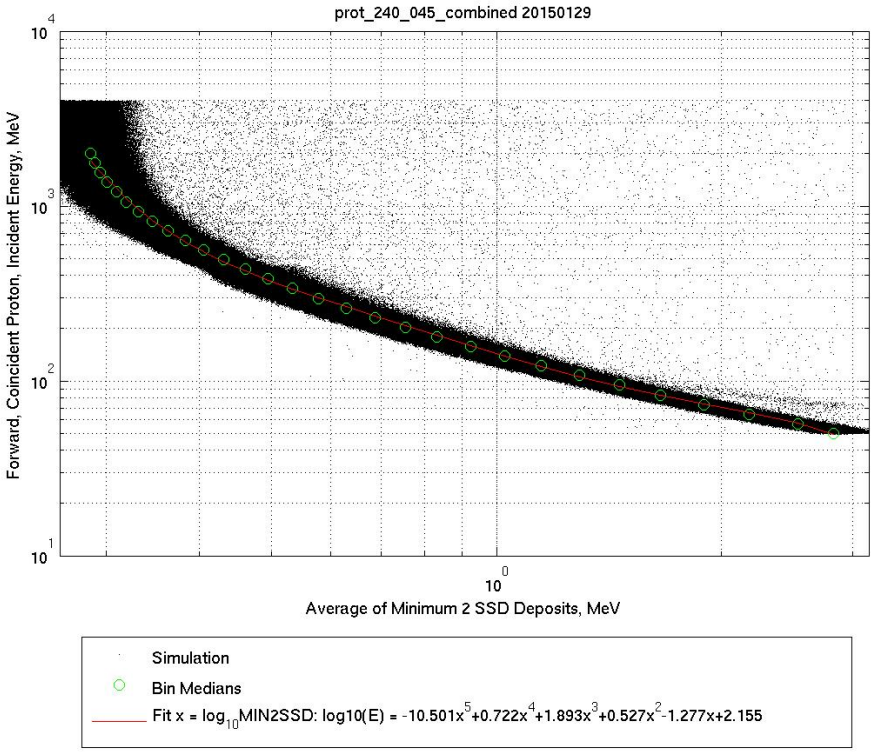

Figure 4. Geant4 simulation and MIN2SSD energy assignment fit.

For posterity, we explored two alternate energy determination formulas: one based on average of all eight SSD deposits (SSDA) and one based on the Cherenkov photon count (CHE). These are given below:

$$E_{SSDA}(\text{MeV}) = m_1 x^{-m_2} + m_3$$
$$x = \frac{1}{8}\sum_{i=1}^{8} D_i\,(\text{MeV})$$
$$m_1 = 123.654926$$
$$m_2 = 2.0034132$$
$$m_3 = 45.5652124$$

$$\log_{10} E_{CHE}(\text{MeV}) = \sum_{i=0}^{9} b_i x^i$$
$$x = \frac{\log_{10}\phi - \mu_1}{\mu_2}$$
$$\mu_1 = 2.1087419721$$
$$\mu_2 = 0.38347690680$$
$$b_0 = -0.051087979473$$
$$b_1 = 0.012900312828$$
$$b_2 = 0.37739175773$$
$$b_3 = -0.10470519644$$
$$b_4 = -0.92420158399$$
$$b_5 = 0.36861849413$$
$$b_6 = 0.83185319936$$
$$b_7 = -0.45375287738$$
$$b_8 = 0.044067338299$$
$$b_9 = 2.7040041153$$
$$\phi = \text{Cherenkov photons counted}$$

5. Flux Conversion Factors

RPS telemeters direct event data (SSD and Chereknov data) for every particle that meets the sensor's coincidence criteria. After background events are filtered out, the foreground events are channelized on the ground into 20 energy bins based on the computed MIN2SSD energy. The 20 channels edges are defined, in MeV, as follows: 0, 70, 82, 95, 111, 130, 151, 176, 206, 240, 279, 326, 380, 443, 516, 602, 702, 818, 964, 1112, ∞. That is, the first channel accepts any event identified as having an energy below 70 MeV, and the last channel accepts any event identified as having an energy above 1112 MeV. These channels are logarithmically spaced.

Because the background rejection is imperfect and the MIN2SSD energy assignment is imperfect, we must develop an algorithm to convert between observed counts in each channel to the implied proton flux at some associated energy. The Geant4 simulation provides full 3-D (energy, angle, angle) responses for every channel, and a spectral inversion would be possible. However, such inversions are not particularly practical for routine processing. Instead, we use a bowtie analysis [8][5], which provides simple flux conversion factors. In a bowtie analysis, we determine the effective energy center and flux conversion factor for each channel based on how many counts that channel would register for a set of typical spectral shapes expected in the inner zone.

In our bowtie analysis, we assume power-law spectra of the form E^{-n} with exponents $n = 2, 2.5, \ldots 4$. These are consistent with energy spectrum analysis using preliminary flux conversion factors from RPS based solely on nominal channel energy bandwidths and geometry and assumption of 100 percent detection efficiency, as well as a version of the AP9 model that was produced before RPS data were available [1]. Figure 2 shows several inner zone spectra from RPS itself and from the AP9 model with E^{-2} and E^{-4} traces superimposed.

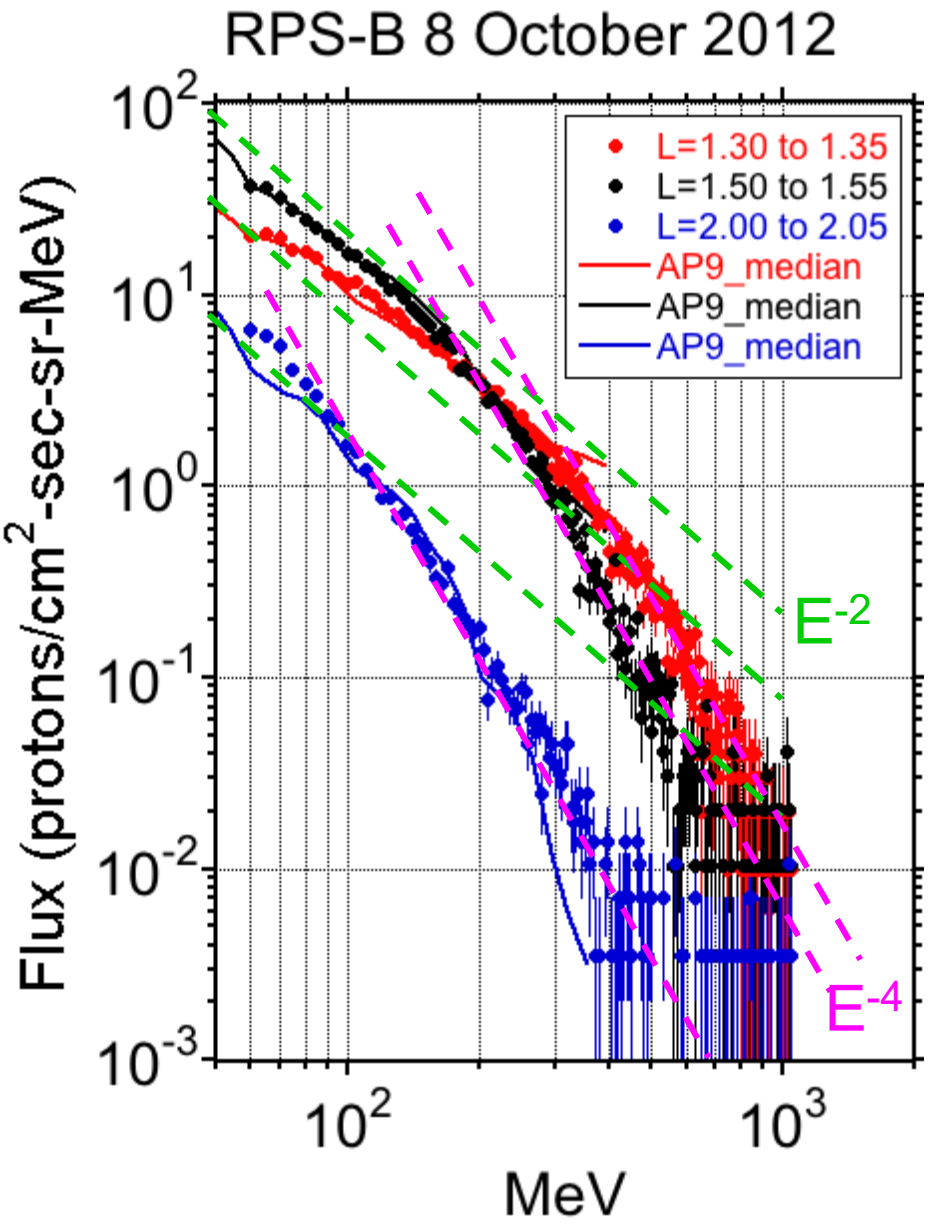

Figure 5. Justification of choice of E^{-2} to E^{-4} spectra for RPS based on preliminary flux conversion factors and an early version of the AP9 model.

Using the Geant4 simulation, we can compute the omnidirectional response function $R(E)$ for RPS. For an assumed isotropic spectrum $j(E)$, the expected count rate is:

$$r = \int_0^\infty R(E)j(E)dE$$

The goal of the bowtie analysis is to approximate this integral with an implied delta function, an idealized differential energy channel:

$$r = \int_0^\infty R(E) j(E) dE \approx j(\bar{E}) \overline{G\delta E}$$

The bowtie analysis deduces the effective energy $\bar{E}$ and the flux conversion factor $\overline{G\delta E}$. If the bowtie analysis is successful, the flux at E_0 can be computed from the observed rate as:

$$j(\bar{E}) \approx \frac{r}{\overline{G\delta E}}$$

To perform the bowtie analysis, we integrate the response function $R(E)$ with the candidate spectrum, and denote this integral $\hat{r}_n$, for which:

$$\hat{r}_n = \int_0^\infty R(E) E^{-n} dE \approx \bar{E}^{-n} \overline{G\delta E}$$

For each candidate spectrum, we have a relationship between the flux conversion factor $\overline{G\delta E}$ and the effective energy $\bar{E}$.

$$\overline{G\delta E} \approx \frac{\bar{E}^{-n}}{\hat{r}_n}$$

We chose a final effective energy $\bar{E}$ that minimizes the standard deviation of the flux conversion factors across the candidate spectra. We also record that standard deviation as a bowtie error, which we typically express in relative terms (i.e., the standard deviation in $\overline{G\delta E}$ divided by $\overline{G\delta E}$ itself, or, equivalently, the standard deviation of $\ln \overline{G\delta E}$). The bowtie results are stored in the skeleton CDF files used to create all the RPS level 2 and higher-level data products as either FPDU (for unidirectional fluxes) or FPDI (for isotropic, i.e., spin averaged, fluxes) supporting data variables. Table 1 provides the numerical results of the bowtie analysis. Figure 3 plots the response function and bowtie results for all 20 channels. For some middle channels, like P9–P13, the backward proton response creates a second peak, causing the bowtie analysis to produce a wider effective energy bandwidth. For channels P15–P19, the broad response at reduced efficiency causes the bowtie analysis to assign the channel a relatively low energy bandwidth and an effective energy that is well off-center or even below the nominal channel acceptance band. Although the bowtie analysis assigns P20 a nominal energy bandwidth for an effective differential channel, its response function is more like an integral channel. So long as the inner belt spectral shapes remain in the E^{-2} to E^{-4} family assumed in the bowtie analysis, the computed RPS fluxes will be reasonable, with 1-σ relative errors of 7 percent or less, as indicated in Table 1 (except P20, which has errors of 17 percent). However, for cosmic ray or solar proton event fluxes, the spectral shapes could be quite different, meaning specialized flux conversion approaches might be needed for analyses of those data. For these and other applications where the full sensor response would be useful, see [6].

Table 3. Bowtie Analysis Results

Channel	Bowtie Energy ($\overline{E}$) FPDU_Energy, MeV	Bowtie Flux Conversion Factor ($\overline{G\delta E}$) FPDU_GdE, MeV cm^2 sr	Flux Conversion Factor Relative Standard Error ($\mathrm{std}\ln \overline{G\delta E}$) FPDU_Crosscalib_RMSE
P1	58.0624	2.43518	0.0139303
P2	74.8728	1.99721	0.02685
P3	89.9281	2.22414	0.0475025
P4	105.557	2.61334	0.0559682
P5	123.394	3.04675	0.0611831
P6	142.977	3.50343	0.0642286
P7	165.09	4.34367	0.0650037
P8	191.88	5.65629	0.0638337
P9	223.516	7.02663	0.0595822
P10	260.73	8.85664	0.0573045
P11	304.56	11.2915	0.0509025
P12	355.851	13.2097	0.0439678
P13	414.811	15.0534	0.0445097
P14	473.269	13.7781	0.0461287
P15	528.714	9.16366	0.0353371
P16	599.821	8.93475	0.026283
P17	682.562	9.32594	0.0268704
P18	786.82	11.0275	0.036323
P19	906.969	11.3961	0.0515706
P20	1324.56	105.285	0.168396

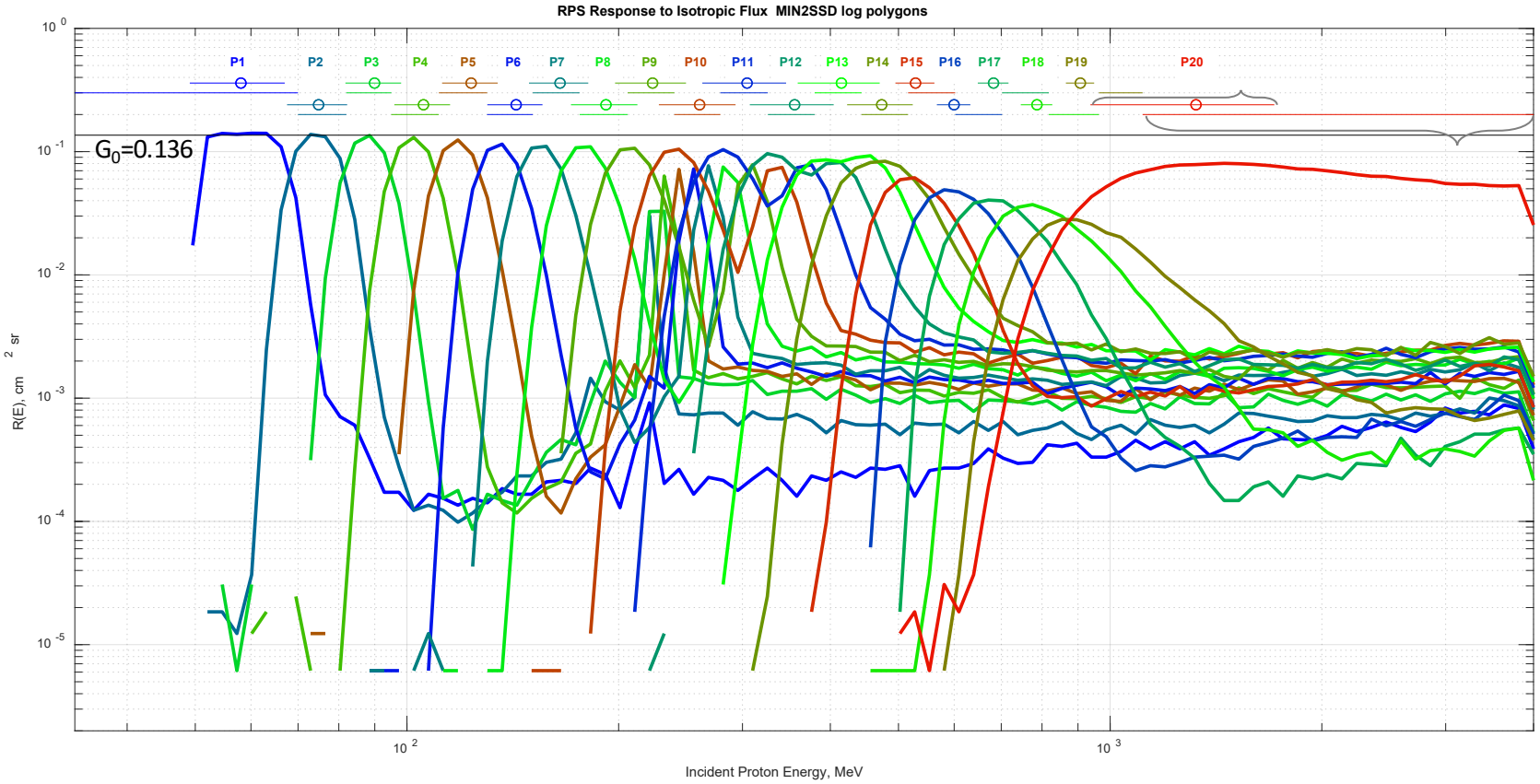

Figure 6. RPS channel responses and bowtie analysis results. A black horizontal line is provided at the nominal RPS geometric factor of $\boldsymbol{G_0 = 0.136}$ cm^{2}sr. Horizontal lines with circles indicate the bowtie effective energy $\overline{\boldsymbol{E}}$ and effective energy bandwidth $(\overline{\boldsymbol{G\delta E}})/\boldsymbol{G_0}$. Horizontal lines slightly below those indicate the range of MIN2SSD energies accepted into the channels. Thick colored traces provide the individual channel omnidirectional responses from the Geant4 simulation.

6. Deadtime and Quota Corrections

The final step in calculating flux is correction for deadtime and quota. Deadtime arises while the sensor processes the charge liberated by particles passing through it. Quotas arise from limitations in the amount of telemetry allocated to RPS and the throughput of the telemetry interface between RPS and the spacecraft. To correct for deadtime and quota, one must consider the RPS telemetry packet structure. Every second, RPS produces a rate and housekeeping (RHK) packet, and if particles were detected meeting all of the coincidence criteria, RPS may also produce a direct event (DE) packet. The structure of these packets is given in [3]. The RHK packets consist of a variety of diagnostic data as well as supporting information needed to assemble the proton flux. The DE packets contain a list of pulse heights and a fine time tag for each event collected during the second.

Deadtime is tracked and reported by the sensor. It is reported on a 16-second multiplex and so must be demultiplexed, time shifted, and interpolated for use in flux determination. The demultiplexed (but not time shifted) value is reported in the level 1 data as DEADTIME_FRACTION. We will denote the time-shifted, time-interpolated deadtime in seconds as d_T, where capital T denotes a particular second.

The RPS sensor separately tracks coincidence rates for PEN (8-fold) and CHE (9-fold) events and reports these every second. We denote these $r_T^{(\mathrm{PEN})}$ and $r_T^{(\mathrm{CHE})}$, respectively, and they are reported in the level 1 data as PEN_RATE and CHE_RATE, respectively. Because there is not enough telemetry to bring down all the direct events, we use separate limits, called "quotas," for PEN and CHE events to allocated telemetry to each type of event. These quotas change with L value by scheduled commands uploaded from the ground. Quotas are denoted $q_T^{(\mathrm{PEN})}$ and $q_T^{(\mathrm{CHE})}$, respectively, and they reported in level 1 data as PEN_QUOTA and CHE_QUOTA, respectively. Table 2 provides a history of the quota L dependence for the two RPS sensors. Figure 7 provides an example L profile of the rates and quotas for a day in the middle of the mission. RPS-B had higher gain in the Cherenkov system, and so had higher CHE rates and needed to use more of its quota for CHE events.

Table 4. RPS Quota Table History

Minimum L	PEN Quota	CHE Quota
RPS-A Commissioning through 13-Sep-2012		
0	100	100
RPS-A 13-Sep-2012 through 5-Feb-2014		
0	120	50
3	10	3
4	1	1
RPS-A 5-Feb-2014 through 25-Nov 2014		
0	300	35
3	10	10
4	7	7
RPS-A 25-Nov 2014 through End of Mission		
0	210	110
3	15	10
4	9	9

Minimum L	PEN Quota	CHE Quota
RPS-B Commissioning through 12-Sep-2012		
0	100	100
RPS-B 12-Sep-2012 through 4-Feb-2014		
0	140	140
3	15	10
4	1	1
RPS-B 4-Feb-2014 through End of Mission		
0	210	110
3	15	10
4	9	9

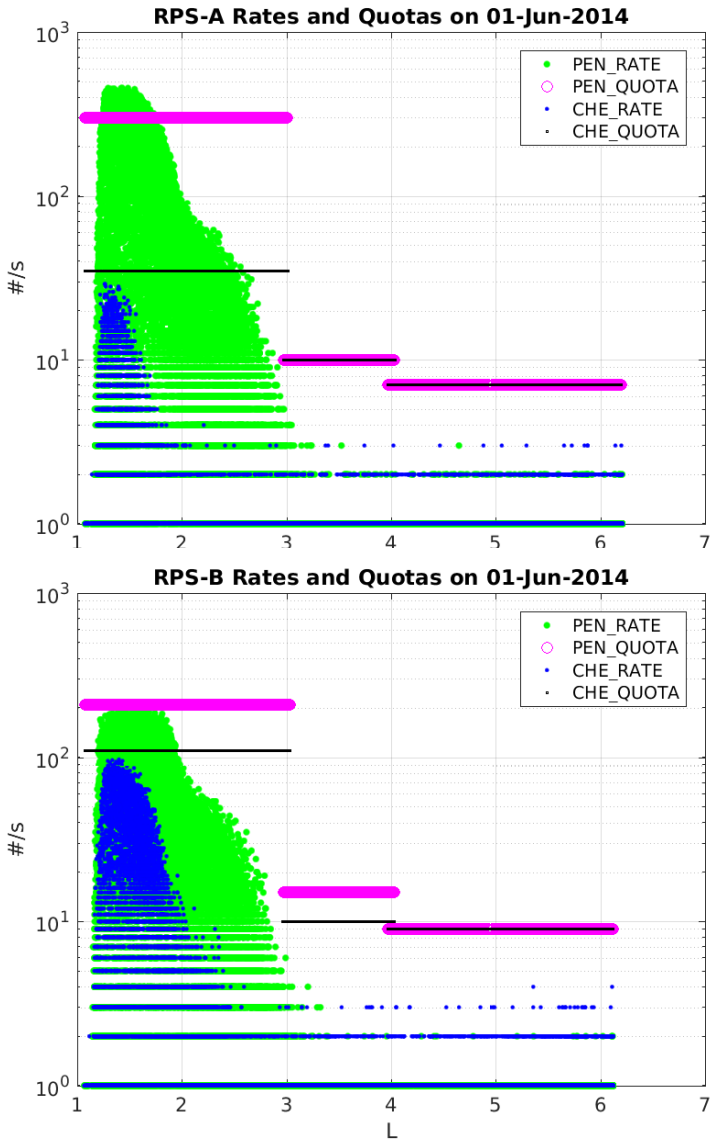

Figure 7. Sample rates and quotas for RPS-A and RPS-B in the middle of the Van Allen Probes mission.

During level 1 processing, an attempt is made to identify each direct event as a PEN event or a CHE event. If the number of events in the DE packet does not match the number expected based on the PEN and CHE rates in the RHK packet, the packet is flagged as having unknown events in it. Any event containing 3 or more pulse heights of 0 or 1 is flagged as invalid – this is a rare artifact of some unknown behavior in the sensor processor.

In some cases, the one-second records are not valid, and this is indicated by values in a bitmask level 1 variable called FLAG. A one-second record cannot be used for flux determination if any of the following is true:

- The sensor is in Alpha Mode (coincidence is disabled)
- The DE packet contains an event marked invalid or unknown
- A DE packet was expected but is missing
- The high voltage is out of range and no correction has been applied for the failed Cherenkov system (correction only available on RPS-A)

6.1 Spin-Averaged Flux Calculation

During level 1 processing, forward events (EVENT_DIRECTION=0) are accumulated into the 20 energy channels producing a 1-second time series $C_{i,T}$, stored in the level 1 data as DATA_CHANNEL_COUNTS. This counts-per-second time series can be converted to a one-second flux on a channel-by-channel basis by accounting for a quota factor Q_T, deadtime d_T, and the bowtie flux conversion factor $\overline{G\delta E_i}$:

$$j_{i,T}^{(\mathrm{second})} = \frac{Q_T C_{i,T}}{\overline{G\delta E_i}(1-d_T)}$$

$$Q_T = \frac{r_T^{(\mathrm{PEN})} + r_T^{(\mathrm{CHE})}}{\max\left(1, \kappa_T^{(\mathrm{PEN})} + \kappa_T^{(\mathrm{CHE})}\right)}$$

The numerator of Q_T is the true number of particles counted, while the denominator is the number telemetered, which is all that can contribute to $C_{i,T}$. The number of events telemetered in each category is the number kept, which is the lesser of the quota or the rate:

$$\kappa_T^{(\mathrm{PEN})} = \min\left(r_T^{(\mathrm{PEN})}, q_T^{(\mathrm{PEN})}\right)$$
$$\kappa_T^{(\mathrm{CHE})} = \min\left(r_T^{(\mathrm{CHE})}, q_T^{(\mathrm{CHE})}\right)$$

Note that because the PEN and CHE events use different quotas, they have different rates of dead time, producing an energy-dependent dead time. This energy dependence is not mitigated by the spin-averaged flux calculation. Because RPS-A and RPS-B have different quota values, their spin-averaged fluxes do not agree as well as their sectored fluxes (next section), which fully account for quota-related dead time.

The one-minute, spin-averaged flux is the arithmetic average of one-second fluxes from the seconds with valid data:

$$j_{i,T}^{(\text{minute})} = \frac{1}{N_{\text{valid}}} \sum_{T\ \text{valid}} j_{i,T}^{(\text{second})}$$

In the level 2 files, this is denoted FPDI, for flux, proton, differential, isotropic, with units #/cm^2/sr/MeV/s. We identify it as an isotropic rather than omnidirectional flux because (1) it does not account for the anisotropic angular distribution and (2) it is expressed per steradian (sr).

We also record the one-minute livetime as a level 2 variable SECONDS, and that is simply the sum of $(1 - d_T)$ for all valid seconds in the minute.

Finally, we compute an error estimate for the one-minute flux as:

$$\text{std ln}\, j_{i,T}^{(\text{minute})} = \sqrt{\frac{1}{1 + \sum_{T\ \text{valid}} C_{i,T}} + \left(\text{std ln}\, \overline{G\delta E_i}\right)^2}$$

This is the standard deviation (std) of the error in the natural log of the one-minute flux. It is a root-mean-squared sum of Poisson error and the bowtie error. This error estimated is stored in the level 2 data as FPDI_RMSE.

6.2 Sectored Flux Calculation

The sectored flux calculation is considerably more complex because it computes flux on timescales less than a second: 1/73rd of a spin for 73 angular sectors. Because it is angle-resolved, the sectored flux is the basis of all higher-level flux products, like pitch angle distributions (level 3) and global flux maps (level 4). At the nominal spin rate of 5.5 rpm, there are approximately 6 2/3 sectors per second, and each sector is about 150 msec long. A sector spans just under 5 degrees. We chose 73 sectors per spin to interlace the local pitch angles with the sectors, whereas a 72-sector division would produce exactly 5 degrees per spin. We note that for RPS, pitch angle is defined as the angle between the magnetic field vector and the incoming particle's momentum (not the sensor field-of view central axis, which points out of the sensor).

Within each sector, it is possible for the quota system to cause RPS to be alive for only a portion of the sector time. RPS can end early, start late, or have a gap of quota-related dead time that splits the sector into two segments of live time. It is also possible for RPS to be "dead" due to quotas for an entire sector. Figure 7 illustrates how the quota live time interacts with the one-second boundaries and the sector boundaries as the events are recorded. To assist in the determination of when the quotas were reached, the level 1 data files include LAST_PEN_TIME and LAST_CHE_TIME, which indicate the time of the last event of the corresponding type if the quota was reached.

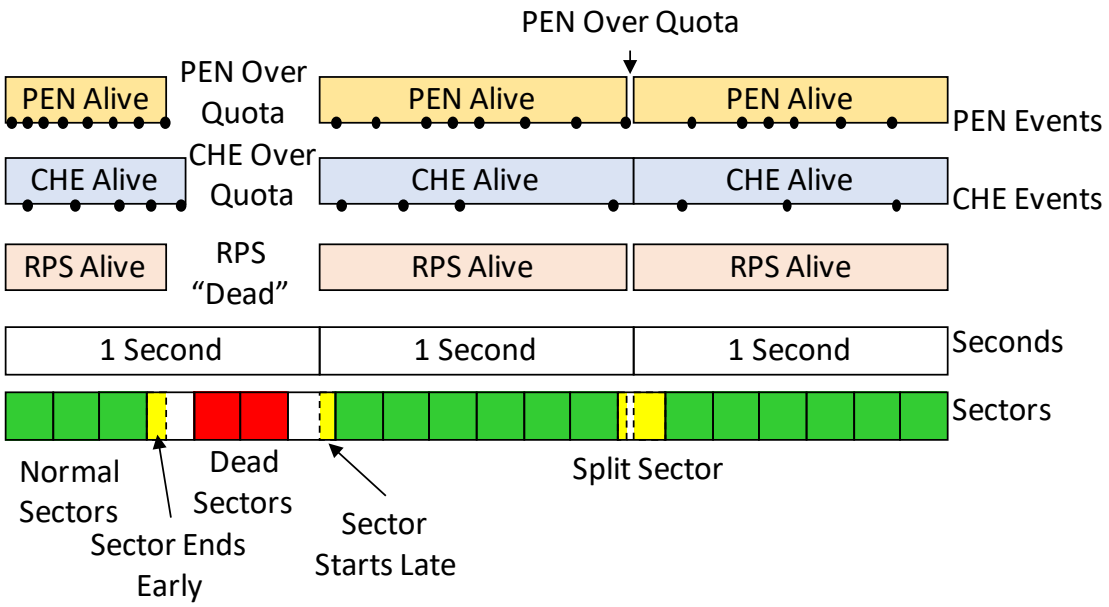

Figure 8. Illustration of the relationship between angular sectors and quotas on one-second packets. Black dots indicate PEN and CHE events. Shaded rectangles indicate live time for PEN and CHE quotas, the RPS sensor itself, and flux accumulation into sectors.

For valid one-second packets, events within each sector are accumulated into counts per channel $c_{i,t}$, and sector livetime τ_t (in seconds) is also accumulated, accounting for sector live time (green or yellow in Figure 7) multiplied by the appropriate sensor deadtime correction $(1 - d_T)$. Note that in a split sector, a different deadtime correction might be used for the first segment than the second segment, which come from different parent one-second packets. The sector flux and its relative standard error are then given by:

$$j_{i,t}^{(\text{sector})} = \frac{c_{i,t}}{\overline{G\delta E_i}\tau_t}$$

$$\text{std ln } j_{i,t}^{(\text{sector})} = \sqrt{\frac{1}{1 + c_{i,t}} + \left(\text{std ln } \overline{G\delta E_i}\right)^2}$$

The flux is stored in the level 2 data as FPDU, for flux, proton, differential, unidirectional, with units of #/cm^2/sr/MeV/s, just like FPDI. The counts $c_{i,t}$ are stored as DATA_CHANNEL_COUNTS, the livetime τ_t is stored as SECTOR_SECONDS, and the error is stored as FPDU_RMSE. SECTOR_START and SECTOR_END time tags are provided to indicate the beginning and end of the sector live time, and the sector time tag itself (EPOCH) is the midpoint between these.

6.3 RPS-A to RPS-B Comparison

To compare RPS-A to RPS-B, we examine level 2 fluxes for calendar year 2015. We compute OPQ *L*-binned fluxes in 0.1 *L* bins from 1.15 to 1.85, where inner zone proton fluxes are most intense. For the spin-averaged product (FPDI), we average fluxes when the locally mirroring particles have an equatorial pitch angle of 85° or more. For the sectored product (FPDU), we use sectors with a boresight equatorial pitch angle of 85° or more. These *L* and pitch angle limits remove most of the orbital differences between the two satellites. Figure 9 shows that for energies up to about 500 MeV, the RPS-A instrument reports FPDU fluxes about 20 percent lower than the RPS-B instrument and about 40 percent lower in the FPDI product. Above 500 MeV, the disagreement is about half as large. Since the FPDU product accounts for

the relative quotas between PEN and CHE events and the FPDI product does not, it is the more accurate of the two. Thus, the RPS absolute accuracy is estimated to be on the order of 20 percent below 500 MeV, and 10 percent above 500 MeV.

Another way to compare RPS-A and RPS-B is during a close physical conjunction. Figure 10 shows two such cases near L~1.45 and near the magnetic equator, when the vehicles were separated by about 500 km. Because RPS has significant Poisson noise, these data have been averaged over two minutes but restricted to times when the sensor was nearly perpendicular to the magnetic field. The error bars show only Poisson error, since the residual bowtie error is the same for both. Panel (a) shows a comparison before the failure of the RPS-A Cherenkov system (next section), while panel (b) shows the comparison after the failure and correction. In both cases, the two sensors agree with each other within the Poisson error.

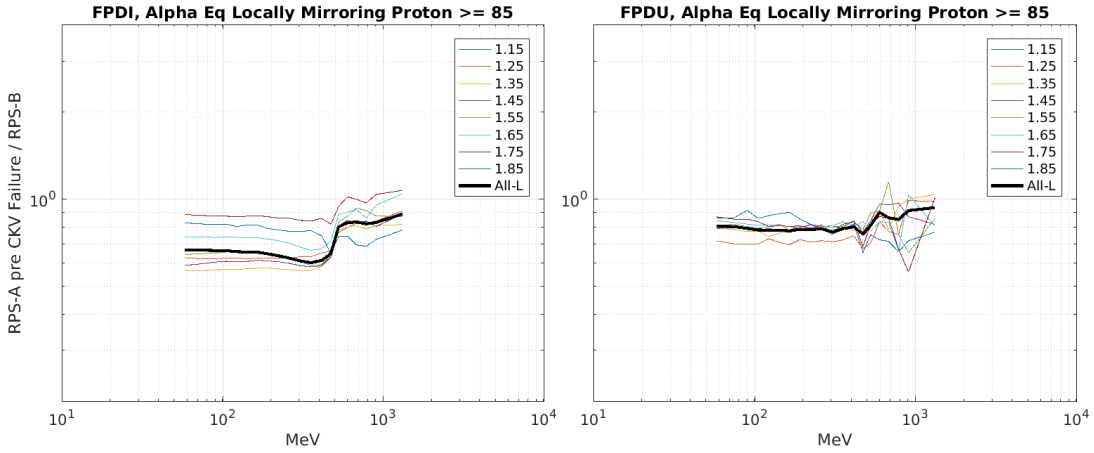

Figure 9. Ratio of equatorial fluxes for RPS-A to RPS-B. Left: spin averaged, right: unidirectional.

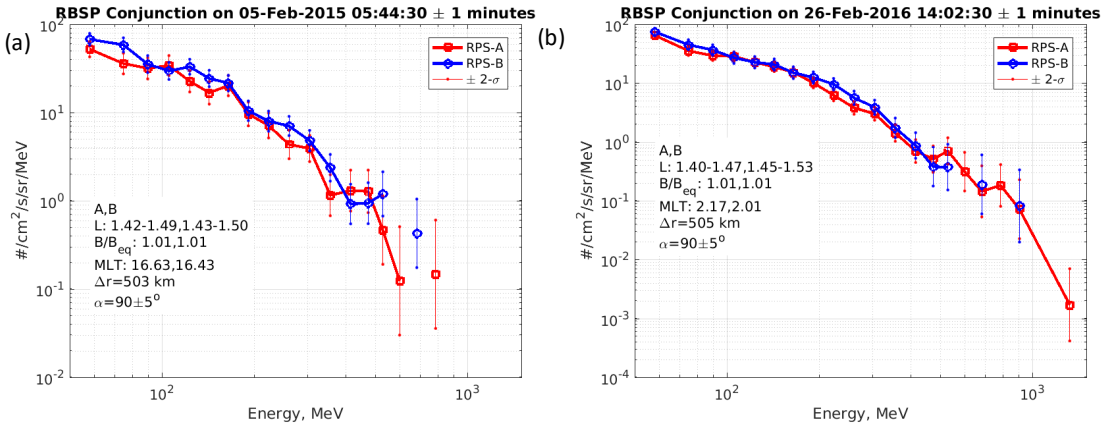

Figure 10. Comparison of RPS-A during conjunction near L~1.45. (a) Before RPS-A Cherenkov failure, (b) after.

7. Backgrounds and Recovering from the RPS-A Cherenkov Failure

RPS is sensitive to high-energy leptons that penetrate all eight SSDs. Both electrons and positrons with about 8 MeV are able to penetrate the SSD stack and begin to produce Cherenkov light. The Cherenkov system removes most of these particles because they do not generate an amount of light consistent with what a proton would, given how much energy they deposit in the SSDs. We use flagging to identify times when leptons (likely electrons) nonetheless contribute to RPS fluxes. Also, the RPS-A Cherenkov system failed on orbit in 2016, limiting our ability to filter the penetrating particles and necessitating new correction and background flagging strategies.

7.1 Lepton Belt Background

An unexpected particle population, identified as >30 MeV leptons, is present on *L* shells 1.5-3.0. This stable population appears as a low-level background in RPS channels P18–P20. Therefore, a data quality flag of 5, indicating possible electron background, is set in both RPS-A and RPS-B in all flux files to indicate this lepton background in the *L*=1.5-3.0 region. A more detailed analysis of pulse height data can reveal more details about the precise location of this presumed lepton belt; this data flag is meant only as a rough indicator of where the contamination exists.

7.2 Flux Recovery from RPS-A Cherenkov Failure

In January 2016, the high voltage on the RPS-A microchannel plate, which counts photons produced by the Cherenkov radiator, began to malfunction. By the 17th, it was deemed unrecoverable. After the Cherenkov failure, we can still compute fluxes, but we have to omit the polygon filter depicted in Figure 3, which relies on the Cherenkov readout. In RPS-A data processing, from January 18, 2016 onward, a correction is applied to allow RPS-A fluxes to be used for non-statistical analysis. These corrected fluxes are less accurate as they have more penetrating backgrounds. **For statistical analysis involving fluxes accumulated over more than a small fraction of a single orbit, RPS-B should be used, since its fully functional Cherenkov radiator allows for more accurate background removal.** The recovered RPS-A fluxes are intended only for use in those studies for which the superior time cadence provided by having two satellites is necessary. Otherwise, RPS-B alone should be sufficient after the Cherenkov failure on RPS-A.

Figure 9 shows an example of fluxes for one day where we computed foreground counts in channels P12 and P14 with and without the Cherenkov polygon filter (Figure 3). In P12 and all channels below 400 MeV, there is essentially no effect from removing the Cherenkov signal. However, above 400 MeV, as seen in P14, there is an excess of counts. The excess counts are approximately proportional to the true counts, with Poisson noise, and there is no significant variation with *L* value. We found that the constants of proportionality are also stable over time.

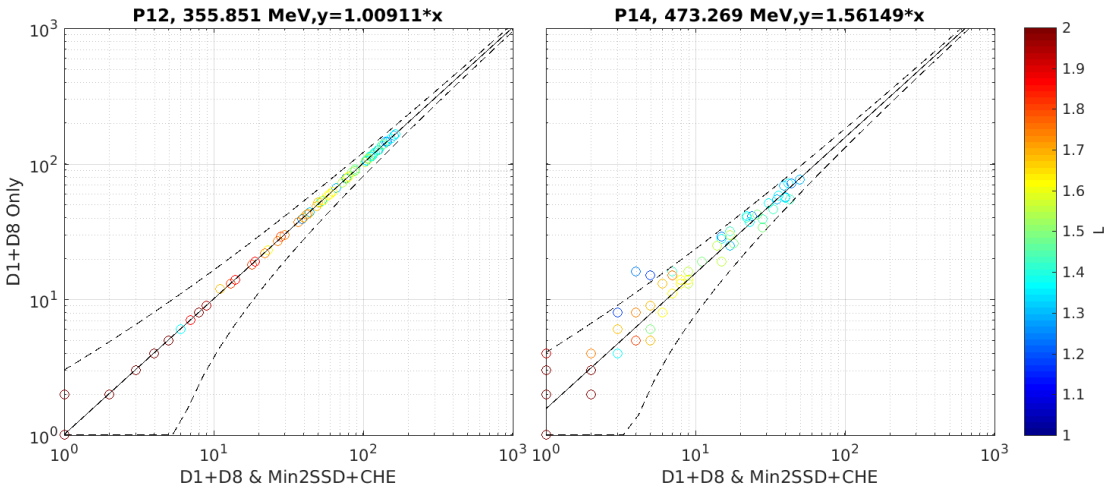

Figure 11. Comparison of counts in two RPS-A channels with (x-axis) and without (y-axis) the Cherenkov polygon filter. Dashed lines depict the expected 95% confidence limits for Poisson noise.

To determine the best correction factor for each channel, we used the same location binning scheme described in section 5.3. We computed the average FPDU flux in each energy channel and *L* bin during 2015 (before the Cherenkov failure) and during the year starting February 1, 2016 (i.e., after the failure). We then computed the before/after flux ratio in each *L* bin for each channel. We adopted as the final correction factor for each channel the average over all *L* bins of the before/after flux ratio. Figure 11 shows the agreement in *L*-binned equatorial fluxes after applying the correction factor for both FPDI and FPDU fluxes. This level of agreement is within the Poisson error of fluxes on a sample-by-sample basis. Longer averages can reveal shortcomings of this simple correction approach. However, for such long averages, as noted above, RPS-B should be used instead. Table 3 provides the multipliers needed to correct the post-Cherenkov failure RPS-A fluxes (i.e., those without the Cherenkov polygon filter). These correction factors are applied as part of the level 2 processing.

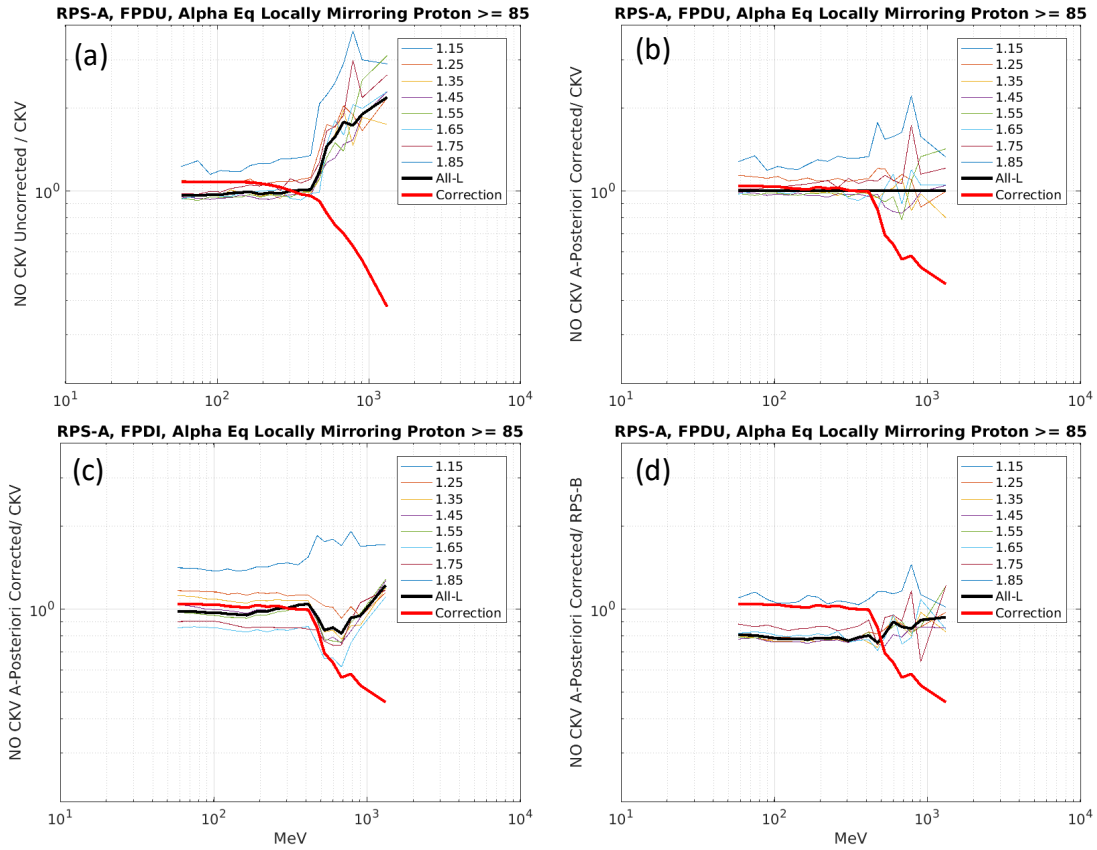

Figure 12. Correction of RPS-A fluxes for excess counts after removal of the Cherenkov polygon: (a) ratio of uncorrected unidirectional equatorial fluxes to pre-failure equatorial fluxes, (b) ratio of corrected fluxes, (c) ratio of corrected spin-average fluxes to pre-failure spin-averaged fluxes, (d) ratio of corrected unidirectional fluxes from RPS-A to RPS-B fluxes.

Table 5. Post-Cherenkov Failure Correction Factors for RPS-A (Multipliers)

P1	P2	P3	P4	P5
1.0409	1.0425	1.0344	1.0350	1.0214
P6	P7	P8	P9	P10
1.0160	1.0088	1.0308	1.0177	1.0246
P11	P12	P13	P14	P15
1.0025	0.99594	0.99119	0.85500	0.69044
P16	P17	P18	P19	P20
0.63761	0.56319	0.58007	0.52740	0.45813

The removal of the Cherenkov polygon filter after the Cherenkov system failure allows outer zone electrons, which penetrate the solid-state detector stack starting at about 8 MeV, to register as valid forward protons. Therefore, after the Cherenkov failure, we introduce a new flagging scheme to indicate the likely presence of significant penetrating electrons (in addition to the stable lepton belt). The daily average PEN+CHE count rate in 0.1 *L* bins is computed, as is the average P1 flux. After the Cherenkov

failure on RPS-A, an *L* bin is suspected of having electron background if the average PEN+CHE count rate exceeds 0.4 #/s and exceeds 20 times the P1 flux in #/cm^2/s/sr/MeV and the center of the *L* bin is greater than 2. For all points in the day between the lowest and highest *L* bins meeting the criteria, the flux data quality flag is set to 5 to indicate possible electron contamination. This is the same flag value used for the lepton belt background indicator. Figure 10 shows an example of this process for channel P19. The lepton background is difficult to see on a daily basis, but when the penetrating outer zone electrons become enhanced, their signature is obvious.

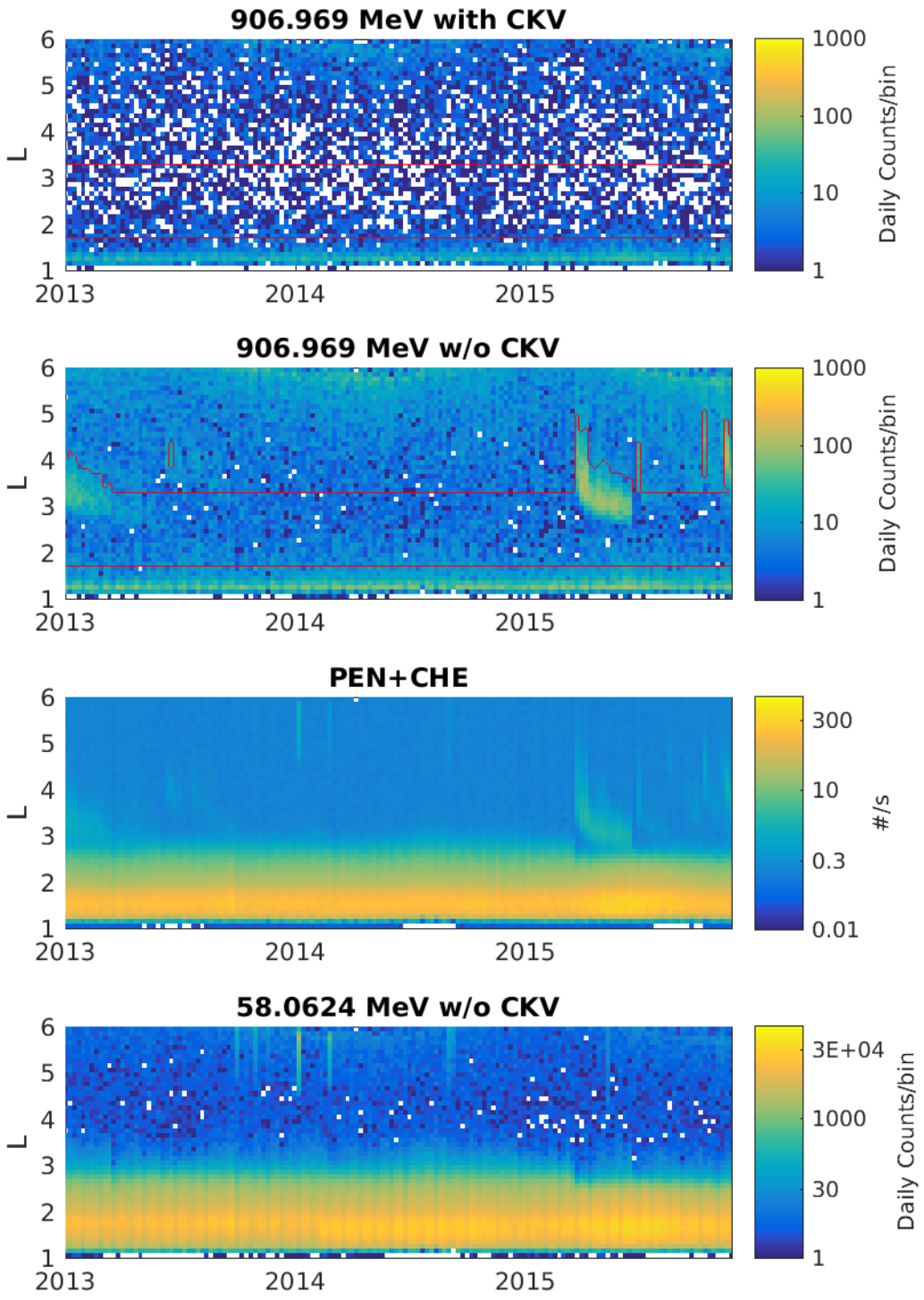

Figure 13. P19 counts in *L*-bins with and without Cherenkov filtering, as well as combined PEN and CHE rates and P1 without Cherenkov filtering. PEN+CHE rates combined with P1 can be used to flag transient outer belt energetic electron contamination. Red traces indicate the boundaries of the electron background flag due to outer and lepton belts.

8. Data Product Overview

RPS has five formal data levels, level 0 through level 4. Table 3 provides a summary of the RPS data products by level. Level 0 data are provided by the mission operations center (MOC) in files containing one full mission day of payload telemetry packets (PTPs). We convert these PTP files to NASA CDF format for wider use. PTP files are broken out by APID: there are separate PTP files for RHK data and for DE data. Final level 0 RHK files follow the naming pattern rbspa_L0-2c1-rh_psbr-rps_YYYYMMDD_vX.Y.Z.cdf, where YYYYMMDD is the universal time (UTC) date of the day most closely matching the nearest mission day, and X.Y.Z is the file version number. DE files follow the corresponding pattern rbspa_L0-2c2-de_psbr-rps_YYYYMMDD_vX.Y.Z.cdf. The RPS sensor was developed as part of an investigation called "Proton Spectrometer Belt Research," and so its filenames contain the acronym psbr. The rbsp acronym refers to Radiation Belt Storm Probes, the original name of theVan Allen Probes mission.

Level 1 data represent the first real processing of the data, in which UTC, calibrations, and coordinates are applied to the data. Level 1 data files merge the RHK and DE data and contain one full UTC day of data. Level 1 and all higher-level data products are available in CDF format. Final level 1 data files follow the naming pattern rbspa_L1_psbr-rps_YYYYMMDD_vX.Y.Z.cdf.

Level 2 data are where fluxes are first computed. There are two types of level 2 data files: 1-minute spin averaged files and sectored files. Level 2 sectored files carry forward direct event data in addition to fluxes. In level 2 files, magnetic coordinates provided by the Energetic Particle Composition and Thermal Plasma Suite (RBSP-ECT) team are included for multiple magnetic field models. Either every minute or every 1/73 spin, a flux spectrum is produced in 20 energy channels. A level 2 file contains one UTC day of data. Final level 2 sectored files follow the naming pattern rbspa_L2_psbr-rps_YYYYMMDD_vX.Y.Z.cdf, and 1-minute files follow the pattern rbspa_L2-1min_psbr-rps_YYYYMMDD_vX.Y.Z.cdf.

Level 3 data consist of one-minute accumulations of flux into three different spin subdivisions: spin sectors, local pitch angle bins, and equatorial pitch angle bins. Equatorial pitch angle is computed in the Olson-Pfitzer Quiet (OPQ) magnetic field model [6], using the local and equatorial values from the model. Every minute, a 2-D table of flux versus energy and angle is produced. A level 3 file contains one UTC day of data. Level 3 files follow the naming pattern rbspa_L3_psbr-rps_YYYYMMDD_vX.Y.Z.cdf.

Level 4 data consist of daily flux maps on three different coordinate systems: E-K-h_{min}, E-K-Phi, and E-Alpha_Eq-L_m. *E* is particle energy, *K* is the modified second adiabatic invariant (an indicator of motion along the magnetic field direction), h_{min} is the minimum altitude the particle reaches in its motion around Earth, *Phi(Φ)* is the third adiabatic invariant (amount of magnetic flux enclosed by the particles azimuthal drift around Earth), *Alpha_Eq*(α_{eq}) is the equatorial pitch angle, and L_m is the McIlwain *L* value (a radius-like coordinate related to the third invariant). Every day, a 3-D table of flux is produced in each of these three coordinate systems according to the OPQ magnetic field model. Note that there is a one-to-one mapping between Phi and L*, the third invariant. Level 4 files are computed from level 2 data. Each level 4 file contains one UTC month of data. Level 4 files follow the naming pattern rbspa_L4_psbr-rps_YYYYMMDD_vX.Y.Z.cdf, where YYYYMMDD is the UTC date of the first day of data in the file. There is also a level 4 product averaged by orbit leg, rbspa_L4-byleg_psbr-rps_YYYYMMDD_vX.Y.Z.cdf, containing one month of data per file.

Table 6. Summary of RPS Data Products

Data Level	Name	Contents
0 (L0)	Level 0 Data	RPS PTP/CCSDS packets (decoded in CDF version, includes raw space weather data)
1 (L1)	Level 1 Data	Nearly all L0 data, UTC, energy/photon deposits, singles and coincidence rates, s/c location, RPS boresight vector, magnetic field vector, estimated incident energy/angle, dead times (including quota effects), space weather products
2 (L2)	Energy Spectra	UTC, flux versus energy spectrum (once per ~5 degrees rotation), pitch-angle and full magnetic coordinates, direct events
3 (L3)	Energy-Angle Spectra	UTC, energy-pitch angle spectrum (once per minute), magnetic coordinates
4 (L4)	Global Maps	UTC, flux vs $E/\alpha_{eq}/L_m$, flux vs $E/K/\Phi$, flux vs $E/K/h_{min}$, (once per day, once per orbit leg)

RPS fluxes have associated data quality flags listed in Table 7. When generating level 3 and level 4 fluxes, quality flags of 0 and 5 are always kept, while flag of 1 is kept when outside the inner zone (L>2).

Table 7. Flux Quality Flags Used by RPS

Quality Flag	Meaning	Kept in L3, L4 Averages
0	Highest quality	YES
1	Problem with time resolution (large dead time)	L>2
2	Contamination (unused)	NO
3	Saturation (unused)	NO
4	Other problem (unused)	NO
5	Possible electron (lepton) background. Lepton belt and outer-zone penetrating electrons.	YES
10	Not yet quality checked (unused)	NO

9. References

[1] Ginet G. P. et al., "AE9, AP9 and SPM: New Models for Specifying the Trapped Energetic Particle and Space Plasma Environment," Space Sci Rev 179:579-615, DOI 10.1007/s11214-013-9964-y. 2013.

[2] Looper, M. D.; T. P. O'Brien; and J. E. Mazur, *Relativistic Proton Spectrometer Detector Calibration*, Aerospace Report Number ATR-2021-02025, The Aerospace Corporation, El Segundo, CA. 2021.

[3] Mabry, D., *RPS Command and Telemetry Definitions*, PSBR-02003-F, The Aerospace Corporation, July 1, 2011.

[4] Mazur, J. et al., "The relativistic proton spectrometer (RPS) for the radiation belt storm probes mission," Space Science Reviews, 179(1-4), 221–261. https://doi.org/10.1007/s11214-012-9926-9. 2021.

[5] O'Brien T. P.; J. E. Mazur; T. B. Guild; and M. D. Looper, "Using Polar-orbiting Environmental Satellite data to specify the radiation environment up to 1200 km altitude," Space Weather, 13(8):434-445, DOI 10.1002/2015SW001166. 2015.

[6] O'Brien, T. P.; M. D. Looper; and J. E. Mazur, "Sensor Response Files for the Relativistic Proton Spectrometer aboard NASA's Van Allen Probes," zenodo.org, doi:10.5281/zenodo.5502043. 2021.

[7] Olson, W. P., and K. A. Pfitzer, "Magnetospheric magnetic field modeling," Annual Scientific Report, Air Force Office of Scientific Research contract F44620-75-C-0033, McDonnell Douglas Astronautics Co., Huntington Beach, CA, 1977.

[8] Selesnick R. S., and J. B. Blake, "On the source location of radiation belt relativistic electrons," J. Geophys. Res. 105(A2):2607. 2000.

Appendix A. Release Notes for RPS Data

A.1 Data Versioning

All RPS data products carry a version number of the form vX.Y.Z. Different parts of the version name are updated depending on what has changed:

- X: the file contents have changed—variables added, deleted, renamed, resized, retyped
- Y: the processing algorithms have changed in a way deemed significant
- Z: new data has been added, minor changes to the processing algorithms, changes to the metadata

All version 0.Y.Z data is preliminary, as it represents an evolving data processing system. Prior to version 1.0.0, activities that would normally increment the X part of the version number will only increment Y. Therefore, level 0.1.Z and 0.2.0 may contain different variables, etc., whereas normally such a change would promote version 1.Y.Z to version 2.0.0.

Level 4 files

Version 3

- Initial version and post-mission archive

Level 3 files

Version 3

- Initial version and post-mission archive

Level 2 files

Version 3

- Post-mission archive
- Final corrections to metadata
- Final temperature and drift corrections applied
- RPS-A D9 recovery applied
- Improved total dose and dose rate calculation
- Updated metadata to improve ISTP compliance

Version 1.2

- Correction: seconds with no direct events now have zero flux rather than fill
- Inherited L1 v1.2 timing correction on pitch angle determination
- On January 10, 2018, we began reprocessing all level 2 (L2) v1.2 files to fix the length of the SPIN_OMEGA variable. In earlier v1.2 files, it had unit length, but in the reprocessed files, it has the advertised length: the spin rate in rad/s. As this is a change to a minor variable, we are not

incrementing from v1.2 to v1.3. The level 1 (L1) SPIN_OMEGA variables were correct, and so those files are not being reprocessed. This change only affects L2 files.

Version 1.1

- Inherited background removal from L1 v1.1: applied background removal for EVENT_DIRECTION=1 and EVENT_TYPE neither PEN(1) or CHE(2)

Version 1.0

- Changed to byVar compression
- Minor changes to metadata
- After the initial v1.0.0 run, a missing factor of 2pi was discovered in the PHI (3rd invariant) calculation. That is corrected in all files generated after January 1, 2017.
- Note that after January 8, 2016, the RPS-A instrument does not produce any fluxes with our current algorithms due to the failure of the Cherenkov subsystem. A new algorithm is pending.

Version 0.5

- Changed metadata

Version 0.4

- Improved metadata, ISTP compliant

Level 1 files

Version 3.0

- Post-mission archive
- ISTP naming convention
- Final temperature and drift corrections applied
- Added enable mask check
- Updated metadata to improve ISTP compliance
- File names updated to ISTP convention

Version 1.2

- Corrected half-second offset in pitch angle interpolation

Version 1.1

- Applied background removal for EVENT_DIRECTION=1 and EVENT_TYPE neither PEN(1) or CHE(2)

Version 1.0

- Declared v1.0 after additional testing and patching for bad/missing files

Version 0.8

- Changed metadata

Version 0.7

- Improved metadata, nearly ISTP compliant
- Renamed DEADTIME_SECONDS to DEADTIME_FRACTION
- Added flag bit 8 for missing DE packet
- Set PACKET_NUM_SLOTS=0 when PEN_RATE=CHE_RATE=0 and no DE packet

Level 0 files

Version 3.0

- Post-mission archive
- File names updated to ISTP convention
- Updated metadata to improve ISTP compliance

Version 2.1

- Changed metadata

Version 2.0

- Renamed variable DEADTIME_SECONDS to DEADTIME_FRACTION
- Improved metadata

Version 1.0

- Further improved structure of DE files
- Improved metadata
- Enabled compression in CDFs

Version 0.3

- Corrected structure of DE files to have both time series and event series data
- Added some default metadata

Version 0.2

- Recovered some missing packets at end of MET day (affects ASCII only)
- Corrected combined enable mask

Version 0.1

- Changed LIVE* to DEAD*, as in LIVETIME to DEADTIME.
- Populated more global attributes

Version 0.0

- Very experimental. Used to verify data processing and publication chain.

AEROSPACE REPORT NO.
ATR-2021-02018

Relativistic Proton Spectrometer Flux Determination and Data Products

Cognizant Program Manager Approval:

Robert D. Rutledge, DIRECTOR - DEPARTMENT
SPACE SCIENCE APPLICATIONS LABORATORY
PHYSICAL SCIENCES LABORATORIES
ENGINEERING & TECHNOLOGY GROUP

Aerospace Corporate Officer Approval:

Todd M. Nygren, SENIOR VP ENGINEERING & TECHNOLOGY
OFFICE OF EVP

Content Concurrence Provided Electronically by:

T Paul P. O'Brien, SENIOR SCIENTIST
MAGNETOSPHERIC & HELIOSPHERIC SCIENCES
SPACE SCIENCES DEPARTMENT
ENGINEERING & TECHNOLOGY GROUP

Office of General Counsel Approval Granted Electronically by:

Kien T. Le, ASSISTANT GENERAL COUNSEL
OFFICE OF THE GENERAL COUNSEL
OFFICE OF GENERAL COUNSEL & SECRETARY

SY0874

AEROSPACE REPORT NO.
ATR-2021-02018

Relativistic Proton Spectrometer Flux Determination and Data Products

Export Control Office Approval Granted Electronically by:

Angela M. Farmer, SECURITY SUPERVISOR
GOVERNMENT SECURITY
SECURITY OPERATIONS
OFFICE OF THE CHIEF INFORMATION OFFICER

SY0874